Open Access

*Journal of Energy and Power Technology*

LIDSEN Publishing Inc.

Original Research

# Thermo-rechargeable Batteries Fabricated Using Low-cost Materials

Arnold Hendharto Widdhiarta [1], Yousuke Shimaura [1], Ichiro Nagai [2], Takayuki Shibata [3], Yutaka Moritomo [1, 2, 4, *]

1. Graduate School of Pure and Applied Science, University of Tsukuba, Tsukuba, Japan; E-Mails: s2020396@s.tsukuba.ac.jp; s2020169@s.tsukuba.ac.jp; moritomo.yutaka.gf@u.tsukuba.ac.jp
2. Graduate School of Pure and Applied Science, University of Tsukuba, Tsukuba, Japan; E-Mail: nagai.ichiro.ge@un.tsukuba.ac.jp
3. Faculty of Marine Technology, Tokyo University of Marine Science and Technology, Koto-ku, Japan; E-Mail: tshiba0@kaiyodai.ac.jp
4. Tsukuba Research Center for Energy Materials Science (TREMS), University of Tsukuba, Tsukuba, Japan

* **Correspondence:** Yutaka Moritomo; E-Mail: moritomo.yutaka.gf@u.tsukuba.ac.jp

**Academic Editor:** Osamu Yamamoto

**Special Issue**: Battery Materials for Energy Conversion

*Journal of Energy and Power Technology*
2022, volume 4, issue 1
doi:10.21926/jept.2201011

**Received:** February 15, 2022
**Accepted:** March 21, 2022
**Published:** March 30, 2022

**Abstract**

We fabricated three thermo-rechargeable batteries using low-cost transition metal hexacyanoferrate and determined the thermal voltage ($V_{cell}$) and discharge capacity ($Q_{cell}$) per unit weight of the total active material in the cathode and anode. The obtained values were compared with the calculated values, which were determined by analyzing the temperature and capacity coefficients of the redox potential.

**Keywords**

Energy harvesting; tertiary battery; transition metal hexacyanoferrates; low-cost material

## 1. Introduction

Thermal energy harvesting technology is indispensable for the reduction of carbon consumption. Among the various energy harvesting devices in use, the battery-based device is promising because the low-cost mass production of the devices is possible. Recently, numerous researchers have reported that a battery can be charged by heating or cooling [1-11] by exploiting the difference in the temperature coefficients (α) of the redox potential (V) between the cathode and anode. The battery is a kind of thermo-rechargeable battery. In this paper, we label such a battery as a "tertiary battery." The cell voltage ($v_{cell}$) increases from 0 V to $V_{cell}$ (thermal voltage) under conditions of warming while the $v_{cell}$ decreases from 0 V to - $V_{cell}$ under conditions of cooling. The electric energy charged under conditions of heating or cooling works during a discharge process. Like a heat engine, the tertiary battery converts thermal energy to electrical energy during the thermal cycle occurring between low ($T_L$) and high ($T_H$) temperatures. This is in sharp contrast to the function of the secondary battery, which is charged using external power. Similar to the secondary battery, the important performance parameters of the tertiary battery are $V_{cell}$ and discharge capacity ($Q_{cell}$) per unit weight of the total active material in the cathode and anode. This is because the product of $V_{cell}$ and $Q_{cell}$ governs the energy density per unit weight of the total active material. The larger the product, the higher the efficiency of the tertiary battery to convert thermal energy into electrical energy. The thermal voltage is determined by α and is expressed as $V_{cell}^{calc} = (\alpha^+ - \alpha^-)(T_H - T_L)$, where $\alpha^+$ ($\alpha^-$) represents the α of the cathode (anode) material. On the other hand, the discharge capacity is governed by α and the charge coefficient (β) of V and is expressed as $Q_{cell}^{calc} = (\alpha^+ - \alpha^-)(T_H - T_L)/[\ \beta^+/(1-r) + \beta^-/r]$, where $\beta^+$ ($\beta^-$) and r [$= m^+/m^+ + m^-$, where $m^+$ ($m^-$) is the weight of cathode (anode) material ] are β of the cathode (anode) material and the weight ratio of the cathode material [11].

Prussian blue analogs, $Na_xM\ [Fe(CN)_6]_y$ (M-PBAs, where M = Mn, Fe, Co, Ni, and Cu), and $Na_2Zn_3[Fe(CN)_6]_2$ (Zn-HCF) are prototypical transition metal hexacyanoferrates. These compounds were investigated as electrode materials for the fabrication of $Na^+/Li^+$ secondary batteries [12-16]. They are promising electrode materials for tertiary batteries [4-11]. M-PBAs consist of a jungle-gym-type host framework and guest species ($Na^+$ and $H_2O$). The nanopores of the framework reversibly accommodated the guest species for efficient fabrication of batteries. They could also be used for selective ion adsorption and gas storage. Ni-PBA, Fe-PBA, and Cu-PBA containing small $M^{2+}$ exhibit face-centered cubic (fcc) structure ($Fm\bar{3}m$; Z = 4). In the fcc structure, the crystallographic Na site is located at the center of the nanopore. The number (N) of the crystallographic Na site increases with an increase in the ionic radius of the $M^{2+}$ ion [17]. On the other hand, Zn-HCF [18-20] consists of a zeolite-like host framework and guest species in a trigonal structure ($R\bar{3}c$; Z = 6). Importantly, the α values of these compounds significantly depend on M, and the values range from -1.18 mV/K in Cd-PBA to 0.57 mV/K in Co-PBA [17]. The material dependence of α can be ascribed to the material dependence of the redox site and N. The resultant material-dependent constraint depends on the $Na^+$ configuration.

To date, the performance of the tertiary batteries made of transition metal hexacyanoferrates, such as the Co-PBA/Ni-PBA [10, 11], Co-PBA/Mn-PBA, Co-PBA/Cu-PBA, and Co-PBA/Zn-HCF have been investigated [11]. The disadvantage of these tertiary batteries is that Co and Ni are relatively expensive elements. It is desirable to develop tertiary batteries using materials composed of only cheap metal elements, such as Fe, Cu, and Zn. Among the transition metal hexacyanoferrates, Fe-PBA, Cu-PBA, and Zn-HCF are composed of cheap metal elements. In addition, the synthetic cost of

Fe-PBA, Cu-PBA, and Zn-HCF are low because they are easily synthesized in an aqueous solution at room temperature.

In this study, we determined the $V_{cell}$ and $Q_{cell}$ of tertiary batteries made of low-cost transition metal hexacyanoferrates ($Na_xFe$ $[Fe(CN)_6]_{0.89}3.8H_2O$ (Fe-PBA), $Na_xCu$ $[Fe(CN)_6]_{0.88}5.8H_2O$ (Cu-PBA), and $Na_xZn_3[Fe(CN)_6]_{1.96}7.2H_2O$ (Zn-HCF)). We compared the observed $V_{cell}$ and $Q_{cell}$ values with the calculated $V_{cell}^{calc}$ and $Q_{cell}^{calc}$ values.

## 2. Materials and Methods

### *2.1 Sample Preparation*

Fe-PBA, Cu-PBA, and Zn-HCF were synthesized following the protocols reported in the literature [17]. The aqueous solution I was slowly dipped into aqueous solution II at a speed of 100 mL/h at 40 °C. The solution I contains 10 mM of $MCl_2$ and 4 M of NaCl, whereas solution II contains 10 mM of $Na_4[Fe(CN)_6]$ and 4 M of NaCl. The mixture was stirred at 40 °C for 12 h. The synthesized powder was filtered, washed, and dried. Figure 1(a) shows the synthesized Fe-PBA, Cu-PBA, and Zn-HCF powders. The chemical composition of the metal elements was evaluated using a scanning electron microscope (SEM: JST-IT 200; JEOL, Ltd.) equipped with an energy-dispersive X-ray spectrometer (EDS). The content of the crystal water was evaluated using a CHN organic elementary analyzer. To investigate the crystal structure, X-ray diffraction (XRD) patterns were investigated using an X-ray diffractometer (MultiFlex; Rigaku). The experiments were conducted at room temperature. The X-ray source was CuKα. In Fe-PBA and Cu-PBA, all the diffraction peaks can be indexed to the fcc cell ($Fm\bar{3}m$; Z = 4). We refined the lattice constant "a" following the Rietveld method (Reitan-FP program [21]): a = 10.275(3) Å for Fe-PBA; a = 10.118(9) Å for Cu-PBA). In Zn-HCF, all the diffraction peaks can be indexed with the trigonal cell ($R\bar{3}c$; Z = 6). We refined the lattice constants (a = 7.430(2) Å and c = 17.526(5) Å) following the Rietveld method.

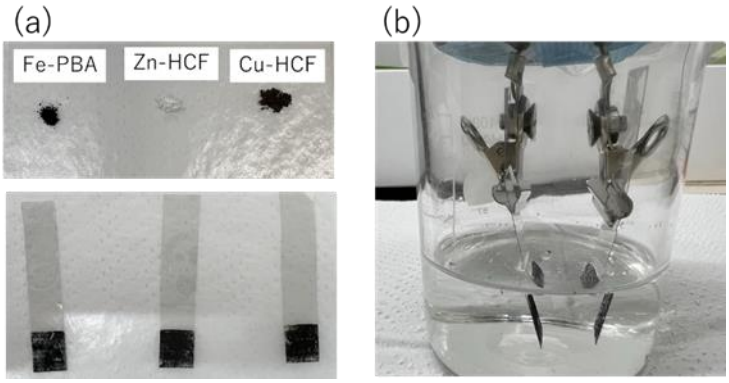


**Figure 1** (a) Synthesized powder (upper) and electrode (lower) corresponding to Fe-PBA, Cu-PBA, and Zn-HCF. (b) Fe-PBA/Zn-HCF tertiary batteries. Fe-PBA, Cu-PBA, Zn-HCF represent $Na_xFe$ $[Fe(CN)_6]_{0.89}3.8H_2O$, $Na_xCu$ $[Cu(CN)_6]_{0.88}5.8H_2O$, and $Na_xZn_3[Fe(CN)_6]_{1.96}7.2H_2O$, respectively.

### *2.2 Electrode Preparation*

The electrodes for Fe-PBA, Cu-PBA, and Zn-HCF were prepared. First, the sample powder, acetylene black, and polyvinylidene difluoride (PVDF) were mixed in the ratio of 7:2:1 with *N*,*N*-

dimethylformamide (DMF). Then, the mixture was pasted on an indium tin oxide (ITO) electrode coated on a polyethylene terephthalate (PET) substrate. The electrode was well dried in a vacuum at 60 °C. The electrodes area was 1.0 $cm^2$. The sample weights for each electrode were in the range of 0.1-0.8 mg. Figure 1(a) shows the electrodes corresponding to Fe-PBA, Cu-PBA, and Zn-HCF. The charge and discharge curves of the electrodes were determined using a potentiostat (HJ1001SD8; HokutoDENKO) in a three-pole beaker-type cell. The sample, Pt, and Ag/AgCl standard electrodes were used as the working, counter, and referential electrodes, respectively. An aqueous solution of $NaClO_4$ (17 mol/kg) was used as the electrolyte. The charge and discharge rates were approximately 0.3 C. The rate was evaluated from the ideal capacity. The current densities are 36.0, 18.2, and 20.1 mA/g for Fe-PBA. Cu-PBA, and Zn-HCF, respectively. The upper and lower cut-off potentials were 1.2 and 0.2 V, respectively, for Fe-PBA, 1.1 and 0.3 V, respectively, for Cu-PBA, and 1.0 and 0.1 V, respectively, for Zn-HCF. The internal resistivity (R) of the electrode was evaluated by analyzing the potential drop against the current density (I <200 mA/g). We confirmed ohmic relation between $V_{drop}$ and I. The tertiary batteries were fabricated with electrodes whose R was less than 0.2 kΩ.

Figures 2 show the first discharge curves of (a) Fe-PBA, (b) Cu-PBA, and (c) Zn-HCF electrodes at 20 °C. The shapes of the discharge curves are consistent with data presented in the literature [12]. The discharge curve corresponding to (a) Fe-PBA exhibits a two-plateau structure. The upper (V = 0.6-0.8 V vs. Ag/AgCl) and lower (= 0.2 V) plateaus were ascribed to the reduction process of $[Fe(CN)_6]^{3-}$ and $Fe^{3+}$, respectively [12]. The discharge curves corresponding to (b) Cu-PBA and (c) Zn-HCF exhibit a single-plateau structure. The observed capacities were ascribed to the reduction process of $[Fe(CN)_6]^{3-}$. We summarized the discharge capacity (Q) and calculated the capacity ($Q^{calc}$). The $Q^{calc}$ values were calculated assuming the redox reactions, $Na_{1.56}Fe^{II}[Fe^{II}(CN)_6]_{0.89}3.8H_2O$ ➔ $Na_{0.56}Fe^{III}[Fe_{II}(CN)_6]_{0.89}3.8H_2O + 1.00\ Na^+ + 1.00\ e^-$ (low-V plateau), $Na_{0.56}Fe^{III}[Fe^{II}(CN)_6]_{0.89}3.8H_2O$ ➔ $Fe^{III}[Fe^{III}(CN)_6]_{0.56}[Fe^{II}(CN)_6]_{0.33}3.8H_2O + 0.56\ Na^+ + 0.56\ e^-$ (low-V plateau), $Na_{1.52}Cu^{II}[Fe^{II}(CN)_6]_{0.88}5.8H_2O$ ➔ $Na_{0.60}Cu^{II}[Fe^{III}(CN)_6]_{0.88}5.8H_2O + 0.88\ Na^+ + 0.88\ e^-$, and $Na_{1.84}Zn^{II}_3[Fe^{II}(CN)_6]_{1.96}7.2H_2O$ ➔ $Zn^{II}_3[Fe^{III}(CN)_6]_{1.84}[Fe^{II}(CN)_6]_{0.12}7.2H_2O + 1.84\ Na^+ + 1.84\ e^-$. The results are presented in Table 1. The observed Q is well reproduced by the calculated $Q^{calc}$.

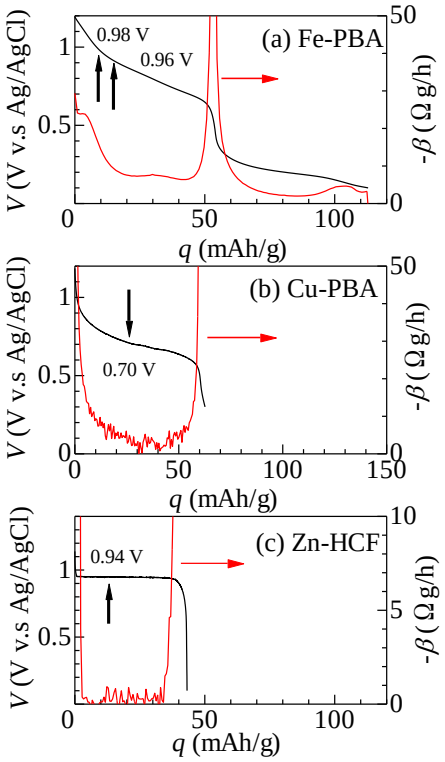


**Figure 2** First discharge curves corresponding to (a) Fe-PBA, (b) Cu-PBA, and (c) Zn-HCF at 0.3 C and 20 °C against capacity (q). The current densities are 36.0, 18.2, and 20.1 mA/g for Fe-PBA. Cu-PBA, and Zn-HCF, respectively. Downward arrows indicate the initial potential of the pre-oxidized electrodes. Thin curves are q-derivatives of the redox potential (V).

**Table 1** Temperature coefficient (α) of V, range of V, discharge capacity (Q), and calculated capacity ($Q^{calc}$) of low-cost transition metal hexacyanoferrates. Fe-PBA, Cu-PBA, and Zn-HCF represent $Na_xFe\ [Fe(CN)_6]_{0.89}3.8H_2O$, $Na_xCu\ [Cu(CN)_6]_{0.88}5.8H_2O$, and $Na_xZn_3[Fe(CN)_6]_{1.96}7.2H_2O$, respectively. In Fe-PBA, the electrochemical parameters for the respective plateaus are listed.

| Compound | α (mV/K) | V (V vs. Ag/AgCl) | Q (mAh/g) | $Q^{calc}$ (mAh/g) |
|---|---|---|---|---|
| high-V plateau of Fe-PBA | -0.16 | 0.60-0.80 | 52 | 43 |
| low-V plateau of Fe-PBA | +0.26[17] | 0.20 | 67 | 77 |
| Cu-PBA | -0.35[17] | 0.70 - 0.90 | 62 | 61 |
| Zn-HCF | -0.83[17] | 0.94 | 43 | 67 |

### *2.3 Determination of α*

The α value corresponding to the high-V plateau of Fe-PBA was determined using a two-pole beaker-type cell connected by a salt bridge. The two electrodes were the same, and they were pre-oxidized to the central position of the high-V plateau. An aqueous solution of $NaClO_4$ (17 mol/kg) was used as the electrolyte. The temperature of one electrode was controlled using a thermos-bath, while the temperature of the other electrode was maintained at room temperature. Voltage difference (ΔV) between the electrodes was measured against the temperature difference (ΔT)

between the electrodes in the open-circuit condition. At each ΔT, we waited for several minutes until ΔV stabilized.

### *2.4 Choice of Cathode and Anode for Tertiary Battery*

Table 1 presents the α values and the range of V corresponding to Fe-PBA, Cu-PBA, and Zn-HCF. Fe-PBA in the low-V plateau exhibits positive α, while Fe-PBA in the high-V plateau, Cu-PBA, and Zn-HCF exhibit negative α. The difference in the sign of α can be ascribed to the difference in the redox sites. The redox site is Fe in the low-V plateau of Fe-PBA, while it is $[Fe(CN)_6]$ in the high-V plateau of Fe-PBA, Cu-PBA, and Zn-HCF [17]. We note that, in a working tertiary battery, the potentials of the cathode and anode should be the same because the thermal cycle operates at approximately 0 V. Usually, the material (or plateau) with positive α, e. g., the low-V plateau of Fe-PBA, is suitable for use as a cathode. However, the potential (V = 0.2 V vs. Ag/AgCl) of the low-V plateau of Fe-PBA significantly deviates from the V ranges of the other materials (or plateaus), i.e., the high-V plateau of Fe-PBA, Cu-PBA, and Zn-HCF. So, we selected the high-V plateau of Fe-PBA as the cathode, as the V range (= 0.6 -0 0.8 V) was close to the range corresponding to Cu-PBA and Zn-HCF. The fabricated Fe-PBA/Cu-PBA and Fe-PBA/Zn-HCF tertiary batteries exhibit finite offset voltages ($V_{off}$) between the cathode and anode. From the viewpoint of performance evaluation, we evaluated the values of $V_{cell}$ and $Q_{cell}$ during the thermal cycle performed around $V_{off}$ as the reference voltage.

### *2.5 Fabrication and Evaluation of Tertiary Battery*

The tertiary batteries were fabricated as two-pole beaker-type cells, whose cathodes and anodes were the pre-oxidized Fe-PBA electrode and pre-oxidized Cu-PBA (or Zn-HCF) electrode, respectively. An aqueous solution of $NaClO_4$ (17 mol/kg) was used as the electrolyte. Both the electrodes were pre-oxidized [4, 10] in the three-pole beaker-type cells (described in sub-section 2.2). Figure 1(b) shows an example of a tertiary battery. Table 2 presents the battery parameters. $\beta^+$ ($\beta^-$), $m^+$ ($m^+$), $R^+$ ($R^-$), and $V^+$ ($V^-$) are the q-coefficient of discharge curve, active material weight, internal resistivity, and initial potential of the cathode (anode), respectively. $V_{off}$ is defined by $V^+$-$V^-$.

The thermal cycle measurements were performed between $T_L$ (= 20 °C) and $T_H$ (= 40 °C) around $V_{off}$. Each cycle consists of four processes, that is, (i) warming, (ii) discharge at $T_H$, (iii) cooling, and (iv) discharge at $T_L$. The temperature (T) of the cell was monitored with a Pt resistance thermometer and controlled in a thermobath. During the process (i), we slowly increased T from $T_L$ to $T_H$ and then maintained the temperature at $T_H$ for 15 min in the open circuit condition. The process increases the cell voltage ($v_{cell}$) from $V_{off}$ to $V_{off} + V_{cell}$. During the process (ii), we allowed the flow of a constant current until $v_{cell}$ reached $V_{off}$. During the process (iii), we slowly decreased T from $T_H$ to $T_L$ and maintained the temperature at $T_H$ for 15 min in the open circuit condition. During the process, $v_{cell}$ was decreased from $V_{off}$ to $V_{off}$-$V_{cell}$. During the process (iv), we allowed the flow of a constant current until $v_{cell}$ reached $V_{off}$. For the convenience of explanation, we will refer to processes (ii) and (iv) as the "discharge" processes.

**Table 2** Parameters of the fabricated tertiary batteries. $\beta^+$ ($\beta^-$), $m^+$ ($m^+$), $R^+$ ($R^-$), and $V^+$ ($V^-$) are the q-coefficient of discharge curve, active material weight, internal resistivity, and initial potential of the cathode (anode), respectively. The β values are determined at 20 °C. $V_{off}$ (= $V^+$-$V^-$) is the offset voltage. The thermal cycle measurements were performed at approximately $V_{off}$.

| Name | Cathode | | | | | Electrolyte |
|---|---|---|---|---|---|---|
| | Material | $\beta^+$ (Wg/h) | $m^+$ (mg) | $V^+$ (mV) | $R^+$ (kW) | |
| Cu1 | Fe-PBA | -16.2 | 0.43 | 960 | 0.20 | 17 mol/kg $NaClO_4$ |
| Cu2 | Fe-PBA | -16.2 | 0.30 | 960 | 0.10 | 17 mol/kg $NaClO_4$ |
| Zn1 | Fe-PBA | -16.2 | 0.36 | 980 | 0.18 | 17 mol/kg $NaClO_4$ |
| name | Anode | | | | | $V_{off}$ (V) |
| | material | $\beta^-$ (Wg/h) | $m^-$ (mg) | $V^-$ (mV) | $R^-$ (kW) | |
| Cu1 | Cu-PBA | -2.1 | 0.15 | 700 | 0.17 | 260 |
| Cu2 | Cu-PBA | -2.1 | 0.22 | 700 | 0.17 | 260 |
| Zn1 | Zn-HCF | -0.2 | 0.78 | 942 | 0.14 | 42 |

## 3. Results

### *3.1 α in the High-V Plateau of Fe-PBA*

Figure 3 shows the ΔV-ΔT plot for the high-V plateau of Fe-PBA. Open and filled circles represent the data obtained under conditions of the ΔT-increasing and ΔT-decreasing runs, respectively. No serious thermal hysteresis was observed in ΔV. We evaluated α following the least-squares fitting (straight line) method. The α value corresponding to the high-V plateau of Fe-PBA was determined to be 0.16 mV/K.

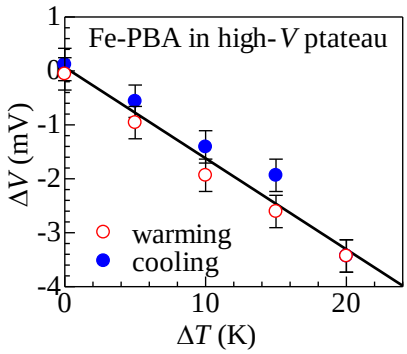


**Figure 3** Voltage difference (ΔV) against temperature difference (ΔT) between cathode and anode. Open and filled circles represent the data obtained in the ΔT-increasing and ΔT-decreasing runs, respectively. The straight line represents the result of the least-squares fitting.

It is interesting that Fe-PBA shows positive α in the low-V plateau and negative α in the high-V plateau region (Table 1). From a thermodynamic point of view, α is expressed as $(S_{re}-S_{ox})/e$, where $S_{re}$ ($S_{ox}$) and e represent the system entropy in the reduced (oxidized) state and elementary charge (>0), respectively. The difference in the sign of α can be ascribed to the difference in the redox sites.

The redox site is Fe ($[Fe(CN)_6]$) in the low-V (high-V) plateau [17]. The reduction process changes the nominal charge ($q_n$) in Fe or $[Fe(CN)_6]$ and modifies the configuration entropy of $Na^+$ near the redox site. A large $|q_n|$ imposes strong restrictions on the Na configuration and reduces the $Na^+$ configuration entropy. In the low-V plateau region, $|q_n|$ (= 2) in the reduced state ($Fe^{2+}$) is smaller than $|q_n|$ (= 3) in the oxidized state ($Fe^{3+}$). Under these conditions, $S_{re}$ is larger than $S_{ox}$, resulting in the generation of positive α, as observed. In the high-V plateau region, $|q_n|$ (= 4) in the reduced state ($[Fe(CN)_6]^{4-}$) is larger than $|q_n|$ (= 3) in the oxidized state ($[Fe(CN)_6]^{3-}$). Under these conditions, $S_{re}$ is smaller than $S_{ox}$, resulting in the generation of negative α, as observed.

### *3.2 Thermal Cycle of Tertiary Battery*

Figure 4(a) presents the cell voltage ($v_{cell}$) of the Cu1 cell during the first thermal cycle between $T_L$ (= 20 °C) and $T_H$ (= 40 °C). A broken straight line represents the offset voltage ($V_{off}$). During the process (i), the cell was slowly warmed from $T_L$ to $T_H$. During this process, $v_{cell}$ increases from 260 mV to 265 mV. During the process (ii) at $T_H$, the cell was discharged at a rate of 0.89 mA/g per unit weight of the total active material. During the process (iii), the cell was cooled from $T_H$ to $T_L$. During this process, $v_{cell}$ decreases from 260 mV to 256 mV. During the process (iv) at $T_L$, the cell was discharged at a rate of -0.89 mA/g. Similar characteristics were observed for the Cu2 [Figure. 4(b)] and Zn1 [Figure. 4(c)] cells. We determined $V_{cell}$ and $Q_{cell}$ during the first thermal cycle and listed the results in Table 3. The tertiary batteries, however, become unstable after the second thermal cycle (results not shown). The change in $v_{cell}$ becomes asymmetric between the warming and cooling processes with an increase in the cycle number. Eventually, the $v_{cell}$ rise in the warming process disappears. Such a deterioration in the thermal cycle is ascribed to the $v_{cell}$ drift toward 0 V with time.

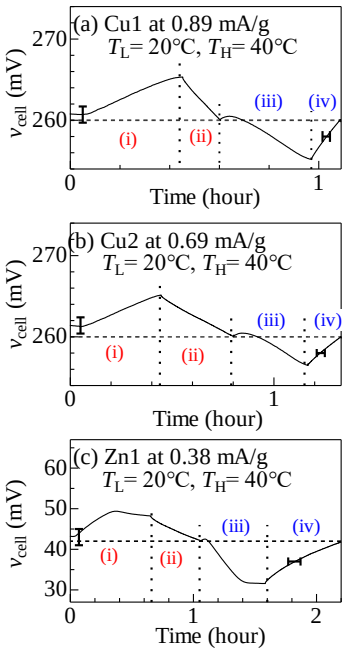


**Figure 4** Cell voltage ($v_{cell}$) of the tertiary batteries during the first thermal cycle between $T_L$ (= 20 °C) and $T_H$ (= 40 °C): (a) Cu, (b) Cu2, and (c) Zn1. Broken straight lines represent the offset voltages ($V_{off}$). The cycle consists of four processes: (i) heating and waiting, (ii) discharge at $T_H$, (iii) cooling and waiting, and (iv) discharge at $T_L$.

**Table 3** Observed thermal voltage ($V_{cell}$) and discharge capacity ($Q_{cell}$) per unit weight of the total active material in the cathode and anode. $V_{cell}^{calc}$ and $Q_{cell}^{calc}$ represent the calculated values. Experimental error in $V_{cell}$ is 1 mV (2 mV) for the Cu1 and Cu2 (Zn1) cells. Experimental error in $Q_{cell}$ is approximately 10%. $V_{cell}^{calc}$ is expressed as $V_{cell}^{calc} = (\alpha^+ - \alpha^-)\,\Delta T$, where $\alpha^+(\alpha^-)$ is the T-coefficient of V for the cathode (anode) material. $Q_{cell}^{calc}$ is expressed as $Q_{cell}^{calc} = (\alpha^+ - \alpha^-)\,\Delta T/[\beta^+/(1-r) + \beta^-/r]$, where $\beta^+$ ($\beta^-$) and r [$= m^+/m^+ + m^-$, where $m^+$ ($m^-$) represents the weight of the cathode (anode) material] are the q-coefficients of V for the cathode (anode) material and the weight ratio of the cathode material. The values above and below slash in the observed columns means values at $T_L$ and $T_H$, respectively.

| name | observed | | calculated | |
|---|---|---|---|---|
| | $\lvert V_{cell}\rvert$ (mV) $T_L/T_H$ | $Q_{cell}$ (mAh/g) $T_L/T_H$ | $\lvert V_{cell}^{calc}\rvert$ (mV) | $Q_{cell}^{calc}$ (mAh/g) |
| Cu1 | 4.7/4.3 | 0.1/0.1 | 4.0 | 0.1 |
| Cu2 | 4.2/4.6 | 0.2/0.1 | 4.0 | 0.1 |
| Zn1 | 5.3/10.3 | 0.2/0.3 | 13.4 | 0.5 |

Figure 5(a) presents the cyclability of the charge and discharge curves corresponding to Fe-PBA (a) at 10 °C and (b) at 50 °C, Cu-PBA (c) at 10 °C and (d) at 50 °C, and Zn-HCF (e) at 10 °C and (f) at 50 °C. The cycle data at 10 °C were obtained using freshly prepared electrodes, while the data at 50 °C were obtained using fully discharged electrodes. The first charge curve corresponding to (a) Fe-PBA at 10 °C presents only the high-V plateau region. This is because Fe is in its trivalent state in the as-grown Fe-PBA system [12]. In (a) Fe-PBA at 10 °C, a small deterioration in the capacity is observed at the $10^{th}$ cycle. The capacity deterioration becomes significant at 50 °C [(b)]. The capacity deterioration at 50 °C may cause the potential drift observed in the tertiary batteries. A comparable capacity at 50 °C is also observed for Cu-PBA [(c) and (d)] and Zn-HCF [(e) and (f)].

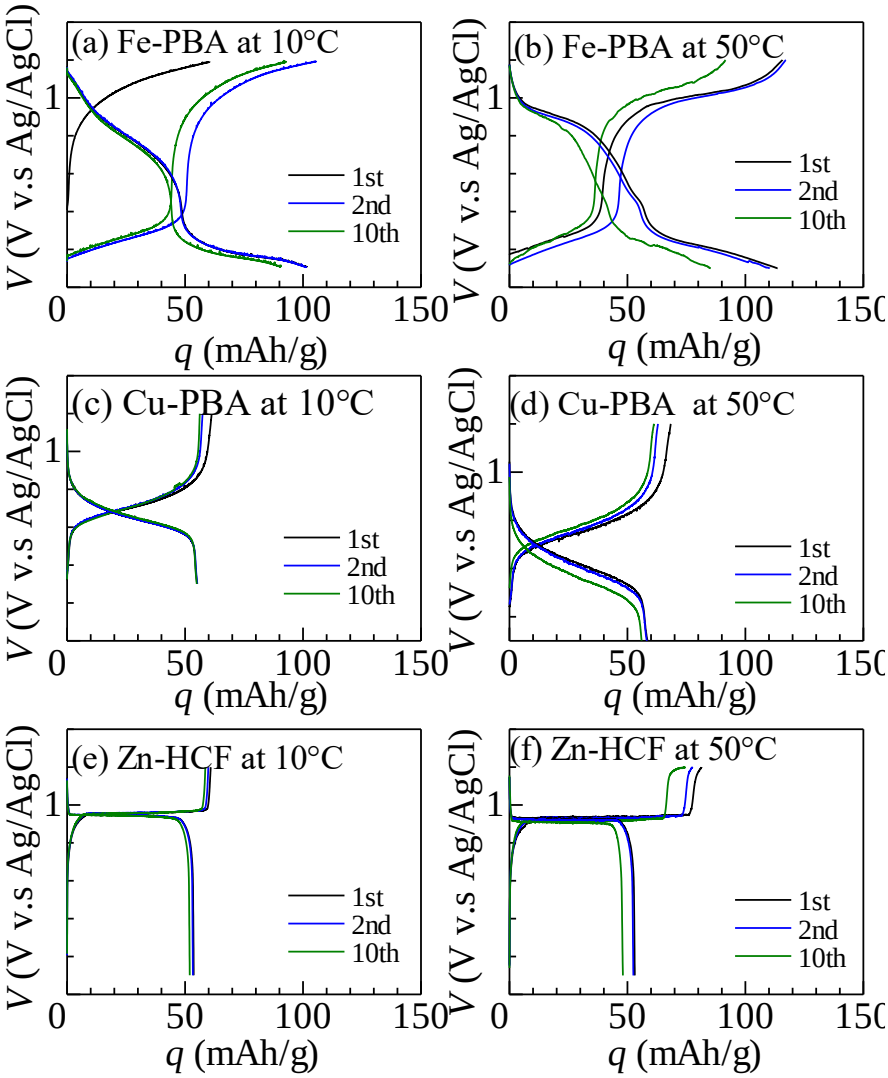


**Figure 5** Cyclability of the charge and discharge curves corresponding to Fe-PBA (a) at 10 °C and (b) at 50 °C, Cu-PBA (c) at 10 °C and (d) at 50 °C, and Zn-HCF (e) at 10 °C and (f) at 50 °C. The cycle data at 10 °C were obtained using fresh electrodes, while the data at 50 °C were obtained using fully discharged electrodes.

## 4. Discussion

Let us compare the observed $V_{cell}$ and $Q_{cell}$ values with the calculated $V_{cell}^{calc}$ and $Q_{cell}^{calc}$ values. $V_{cell}^{calc}$ is expressed as $V_{cell}^{calc} = (\alpha^+ - \alpha^-)\,\Delta T$. In the present experiment, $\Delta T$ is fixed at 20 K. The α values corresponding to Fe-PBA, Cu-PBA, and Zn-HCF are listed in Table 1. $Q_{cell}^{calc}$ is expressed as $Q_{cell}^{calc} = (\alpha^+ - \alpha^-)(T_H - T_L)/[\beta^+/(1-r) + \beta^-/r]$, where r [$= m^+/m^+ + m^-$] is the weight ratio of the cathode material. The β and m values of the investigated cells are listed in Table 2. The calculated $V_{cell}^{calc}$ and $Q_{cell}^{calc}$ values are summarized in Table 3. The observed values have also been presented.

For the case of the Cu1 cell, $V_{cell}$ and $Q_{cell}$ were well reproduced (within the range of acceptable experimental error) by the calculated values. For the Cu2 cell, except for $Q_{cell}$ at $T_L$, $V_{cell}$ and $Q_{cell}$ values were well reproduced by the calculated values (within the acceptable range of experimental error). The high $Q_{cell}$ value at $T_L$ could be attributed to the negative shift in the referential voltage. For the Zn1 cell, the $V_{cell}$ and $Q_{cell}$ values were smaller than the calculated values. The significantly

small $V_{cell}$ value at $T_L$ can be attributed to the drift in the $v_{cell}$ toward 0 V with time. The small $Q_{cell}$ value can potentially be ascribed to the capacity deterioration of Fe-PBA and Zn-HCF at high-temperature conditions.

## 5. Conclusions

We determined the $V_{cell}$ and $Q_{cell}$ values for thermos-rechargeable batteries fabricated from low-cost Fe-PBA, Cu-PBA, and Zn-HCF systems. For the Fe-PBA/Cu-PBA tertiary batteries, the $V_{cell}$ and $Q_{cell}$ values were well reproduced by the calculated values. For the Fe-PBA/Zn-HCF tertiary batteries, the $V_{cell}$ and $Q_{cell}$ values were smaller than the calculated values.

## Acknowledgments

The CNH elementary analyses were outsourced to the Chemical Analysis Division, Research Facility Center for Science and Engineering, University of Tsukuba.

## Author Contributions

Y. S., I. N., and T. S. have set up an experimental base for the tertiary battery research, such as the development of measurement systems and routinization of electrode preparation and tertiary battery fabrication. Y. S. and I. N. characterized the material. A. H. W. fabricated the tertiaries battery and evaluated them. Y. M. made the experimental plan and wrote the manuscript.

## Funding

This work was supported by JSPS KAKENHI (Grant No JP21H01822), Murata Science Foundation, Technova inc., JGC-S Scholarship Foundation, Joint research with Focus Systems Corporation, and Joint research with Taisei Rotec Corporation.

## Competing Interests

The authors have declared that no competing interests exist.

## References

1. Yang Y, Lee SW, Ghasemi H, Loomis J, Li X, Kraemer D, et al. Charging-free electrochemical system for harvesting low-grade thermal energy. Proc Natl Acad Sci. 2014; 111: 17011-17016.
2. Lee SW, Yang Y, Lee HW, Ghasemi H, Kraemer D, Chen G, et al. An electrochemical system for efficiently harvesting low-grade heat energy. Nat Commun. 2014; 5: 3942.
3. Wang J, Feng SP, Yang Y, Hau NY, Munro M, Ferreira-Yang E, et al. Thermal charging phenomenon in electrical double layer capacitors. Nano Lett. 2015; 15: 5784-5790.
4. Shibata T, Fukuzumi Y, Kobayashi W, Moritomo Y. Thermal power generation during heat cycle near room temperature. Appl Phys Express. 2017; 11: 017101.
5. Fukuzumi Y, Amaha K, Kobayashi W, Niwa H, Moritomo Y. Prussian blue analogues as promising thermal power generation materials. Energy Technol. 2018; 6: 1865-1870.
6. Takahara I, Shibata T, Fukuzumi Y, Moritomo Y. Improved thermal cyclability of tertiary battery made of prussian blue analogues. ChemistrySelect. 2019; 4: 8558-8563.

7. Shibata T, Iwaizumi H, Fukuzumi Y, Moritomo Y. Energy harvesting thermocell with use of phase transition. Sci Reps. 2020; 10: 1813.
8. Iwaizumi H, Fujiwara Y, Fukuzumi Y, Moritomo Y. The effect of 3d-electron configuration entropy on the temperature coefficient of redox potential in $Co_{1-z}Mn_z$ Prussian blue analogues. Dalton Trans. 2019; 48: 1964-1968.
9. Shibata T, Fukuzumi Y, Moritomo Y. Thermal efficiency of a thermocell made of Prussian blue analogues. Sci Reps. 2018; 8: 14784.
10. Nagai I, Shimaura Y, Shibata T, Moritomo Y. Performance of tertiary battery made of Prussian blue analogues. Appl Phys Express 2021; 14: 094004.
11. Shimaura Y, Shibata T, Moritomo Y. Interrelation between discharge capacity and charge coefficient of redox potential in tertiary batteries made of transition metal hexacyanoferrates. Jpn J Appl Phys. 2022; 61: 044004.
12. Imanishi N, Morikawa T, Kondo J, Takeda Y, Yamamoto O, Kinugasa N, et al. Lithium intercalation behavior into iron cyanide complex as positive electrode of lithium secondary battery. J Power Sources. 1999; 79: 215-219.
13. Imanishi N, Morikawa T, Kondo J, Yamane R, Takeda Y, Yamamoto O, et al. Lithium interaction behavior of iron cyanometallates. J Power Source. 1999; 81: 530-534.
14. Okubo M, Asakura D, Mizuno Y, Kim JD, Mizokawa T, Kudo T, et al. Switching redox-active sites by valence tautomerism in Prussian blue analogues $A_xMn_y[Fe(CN)_6]\cdot nH_2O$ (A: K, Rb): Robust frameworks for reversible Li storage. J Phys Chem Lett. 2010; 1: 2063-2071.
15. Matsuda T, Moritomo Y. Thin film electrode of Prussian blue analogue for Li-ion battery. Appl Phys Express. 2011; 4: 047101.
16. Takachi M, Matsuda T, Moritomo Y. Structural, electronic, and electrochemical properties of $Li_xCo[Fe(CN)_6]_{0.90}2.9H_2O$. Jpn J Appl Phys. 2013; 52: 044301.
17. Moritomo Y, Yoshida Y, Inoue D, Iwaizumi H, Kobayashi S, Kawaguchi S, et al. Origin of the material dependence of the temperature coefficient of the redox potential in coordination polymers. J Phys Soc Jpn. 2021; 90: 063801.
18. Rodríguez-Hernández J, Reguera E, Lima E, Balmaseda J, Martínez-Garvía R, Yee-Madeira H. An atypical coordination in hexacyanometallates: Structure and properties of hexagonal zinc phases. J Phys Chem Solids. 2007; 68: 1630-1642.
19. Avila M, Rodríguez-Hernández J, Lemus-Santana AA, Reguera E. Cation mobility and structural changes on the water removal in zeolite-like zinc hexacyanometallates (II). J Phys Chem Solids. 2011; 72: 988-993.
20. Avila M, Reguera L, Vargas C, Reguera E. Tetrahedral coordination for Zn in hexacyanometallates: Structures of $Zn_3A_2[M(CN)_6]_2\cdot xH_2O$ with A=K, Rb, Cs and M=Ru, Os. J Phys Chem Solids. 2009; 70: 477-482.
21. Izumi F, Momma K. Three-dimensional visualization in powder diffraction. Solid State Phenom. 2007; 130: 15-20.


Enjoy *JEPT* by:

1. Submitting a manuscript
2. Joining in volunteer reviewer bank
3. Joining Editorial Board
4. Guest editing a special issue

For more details, please visit:
http://www.lidsen.com/journal/jept